ISODRIP, a model to transfer the δ^{18}O signal of precipitation to drip water — implementation of the model for Eagle Cave (central Spain)

Domínguez-Villar, David; Krklec, Kristina; Boomer, Ian; Fairchild, Ian J.

[Link to publication on Research at Birmingham portal](#)

1 **ISODRIP, a model to transfer the δ^{18}O signal of precipitation to drip**

2 **water — Implementation of the model for Eagle Cave (central Spain)**

3

4 David Domínguez-Villar[1]*, Kristina Krklec [1], Ian Boomer[2], Ian J. Fairchild[2]

5

6 [1] Department of Soil Science, Faculty of Agriculture, University of Zagreb, Svetošimunska 25, 10000,

7   Zagreb, Croatia

8 [2] School of Geography, Earth and Environmental Sciences, University of Birmingham, Edgbaston,

9   Birmingham B15 2TT, United Kingdom

10

11 ABSTRACT

12 The isotope signature of cave waters provides an excellent opportunity to better

13 understand the recharge in karst regions and the complexity of drainage systems in the

14 vadose zone. We have developed a cave isotope hydrological model (ISODRIP) that

15 requires entering basic hydrometeorological information and a precipitation δ^{18}O record

16 to simulate the discharge and δ^{18}O signals of different drip sites. The model includes four

17 different modules to simulate various flow route regimes: continuous and discontinuous

18 drips under diffuse or preferential flows. We use precipitation and cave water δ^{18}O

19 records that were obtained in Eagle Cave (central Spain) during a 5-year period to test

20 our model and to better understand the dynamics of karst aquifers. Eagle Cave waters do

21 not record evaporation. The δ^{18}O signals do not have seasonality, although they record

22 intra-annual and inter-annual variability. Additionally, cave water δ^{18}O signal falls within

23 the range of the annual average weighted isotope composition of precipitation. Well-

24 mixed cave waters, that characterize diffuse flows, record 1‰ $\delta^{18}O$ variability, whereas

25 partially-mixed waters, that flow along preferential drainage routes, have up to 3‰ $\delta^{18}O$

26 variability. The results suggest that precipitation takes on average 15 months to reach the

27 cave through the diffuse flow network, whereas under preferential flow the transit time is

28 highly variable depending on the previous condition of the system. ISODRIP includes a

29 soil layer above the vadose zone that controls large recharge events, together with direct

30 recharge components that bypass the soil layer enabling at least some recharge all year

31 round. Thus, the simulations reproduce the observed lack of seasonal bias in the cave

32 water $\delta^{18}O$ composition in relation to the average weighted isotope composition of

33 precipitation. This research highlights the importance of understanding recharge

34 dynamics and the configuration of particular drips sites to properly interpret speleothem

35 $\delta^{18}O$ records.

36

39

40 *Corresponding author at Department of Soil Science, Faculty of Agriculture,

41 University of Zagreb, Zagreb, Croatia. D. Domínguez-Villar, *E-mail address*:

42 ddvillar@hotmail.com

1. Introduction

Signals of climate and environmental conditions that take place over caves are transferred underground, propagated through the bedrock which acts as a filter, and eventually recorded in caves (Fairchild and Baker, 2012). During the transfer process through the vadose zone, the external signal is often smoothed and delayed. The signal transfer depends on several characteristics of the local cave and karst features, but also on the heat or mass transfer processes involved. Thus, a climate or environmental change over a cave that would affect multiple signals (e.g., temperature, amount of precipitation, content of soil CO_2, etc.) may be recorded in the same gallery of the cave at different times, depending on the process that controls the transfer. For example, temperature away from the cave entrances is often controlled by conduction, and climate changes can take from years to millennia depending on the period of the anomaly and the thickness of bedrock over the cave (Moore and Sullivan 1978; Villar et al., 1983; Domínguez-Villar et al., 2015, 2020). On the other hand, air transported underground is frequently dominated by advection, causing a delay of the signal in relation to the surface to be negligible at geological timescales (e.g., Pflitsch et al., 2010; Liñán et al., 2018). In drip waters, the mass transport is affected by both, advective and diffuse transfer processes (Fitts, 2012), and the nature of each flow route imprints singular properties to each drip site (Baker and Fairchild, 2012), affecting the degree of water mixing and the residence time in the vadose zone of karst.

Water isotopes have been traditionally used as tracers to investigate the process of transferring precipitation into caves to better understand underground water flow in the vadose zone of karst regions. Early studies found that in most cases, drip water $\delta^{18}O$

67   values recorded little variability and their average values were close the annual weighted

68   averages of the $\delta^{18}O$ values of precipitation over the caves (Goede et al., 1982; Yonge et

69   al., 1985). Note that the annual weighted average of precipitation multiplies every

70   monthly isotope value by the monthly amount of precipitation, and the sum of those

71   results during the twelve months of the year is divided by the annual precipitation. Thus,

72   the annual weighted isotope composition of precipitation keeps the mass balance. The

73   lack of seasonality in drip water $\delta^{18}O$ signals indicates the mixing of precipitation within

74   the karst and is often used to suggest residence times of the water of at least one year

75   (Ayalon et al., 1998; Fuller et al., 2008; Pape, 2010; Duan et al., 2016). Conversely, the

76   seasonality in drip water $\delta^{18}O$ signals is often used as evidence for residence times shorter

77   than a year (Carrasco et al., 2006; Partin et al., 2012; Breitenbach et al., 2015; Pérez-

78   Mejías et al., 2018). However, even when drip waters record isotope seasonality, those

79   waters are affected by substantial mixing with previous water in the vadose zone,

80   attenuating the amplitude of the annual cycle (Arbel et al., 2010). In addition, the

81   residence time of water in the soil on top of the bedrock can already last several months

82   (Comas-Bru et al., 2015). Studies that have dated drip waters from different cave systems

83   using tritium isotopes have confirmed that the ages of most drip waters range from less

84   than two years to several decades (Even et al., 1986; Chapman, et al., 1992; Kaufmann et

85   al., 2003; Yamada et al., 2008; Kluge et al., 2010; Jean-Baptiste et al., 2019). Tritium-

86   dated waters that are less than one year old have shown no clear seasonality in the drip

87   water $\delta^{18}O$ signal as a result of mixing with previous waters (Even et al., 1986),

88   confirming the importance of water mixing even in the case of dominant preferential flow

89   drip sites. Furthermore, drip water $\delta^{18}O$ seasonality can result from seasonal mixing of

90   underground water reservoirs of different isotopic composition, regardless their residence

91   time (Bradley et al., 2010), an effect also recorded in other proxies such as fluorescence

92   (Domínguez-Villar et al., 2018). Therefore, assessments of residence times based on the

93   structure of the drip water $\delta^{18}O$ signal alone should be taken with caution, since they do

94   not consider the full complexity of the karst hydrology.

95

96   In the last decade, drip water isotope models have helped to understand not only the

97   residence time but also the flow paths of water in the vadose zone of karst terrains above

98   particular drip sites (Baker et al., 2010; Wackerbarth et al., 2010). The complexity of

99   models differs greatly, ranging from simple weighting and mixing calculations to more

100 complex functions that include evapotranspiration and different flow routes (Baker and

101 Bradley, 2009; Wackerbarth et al., 2010; Bradley et al., 2010; Partin et al., 2012; Baker

102 et al., 2012; Treble et al., 2013; Genty et al., 2014; Moerman et al., 2014; Mischel et al.,

103 2015; Markowska et al., 2016; Domínguez-Villar et al., 2018; Jean-Baptiste, et al., 2019).

104 Isotope hydrology models are especially useful in caves where evaporation impact in drip

105 water is negligible. However, in cave systems with low relative humidity (i.e., <<100%),

106 evaporation causes significant isotope fractionation (Bar Matthews et al., 1996; Ayalon

107 et al., 1998; Cuthbert et al., 2014), which is a major control on the drip water $\delta^{18}O$ signal

108 in addition to the precipitation isotope composition. Furthermore, drip water isotope

109 models are very sensitive to periods of water recharge. During periods of severe water

110 deficit, precipitation events may not contribute to the water isotope composition of the

111 deeper sections of those soils. Consequently, the isotope signature of some rainwater

112 events may not be transferred to the vadose zone during recharge events, eventually

113 modifying the weighted average isotope composition of recharge water compared to

114 precipitation. Although precipitation from every month of the year is often required to

115 reproduce the $\delta^{18}O$ signal of drip waters (e.g., Genty et al., 2014), other cave systems

116 seem to record a biased $\delta^{18}O$ signal compared to the weighted average annual $\delta^{18}O$ value

117 of precipitation, because some rain events during the drier portion of the year do not

118 contribute to the drip water $\delta^{18}O$ signal (e.g., Baker et al., 2019). However, soil isotope

119 studies have shown that regardless of recharge being limited to certain events during the

120 year, the isotope composition at the base of the soil, which accounts for most of the

121 recharge, often has an isotope composition that requires contribution of precipitation from

122 all year round (Gehrels et al., 1998; Comas-Bru et al., 2015). In addition, up to now no

123 drip water isotope model with soil layer has accounted for direct recharge: a component

124 of the recharge that by-passes the soil, entering directly to the vadose zone and that is not

125 affected by evapotranspiration.

126 Here we present precipitation and cave water $\delta^{18}O$ records obtained during a 5-year

127 monitoring program in Eagle Cave, a small touristic cavern located in central Spain.

128 Using these isotope records in conjunction with meteorological data and information on

129 the drip hydrology, we developed a transfer function that propagates the $\delta^{18}O$ signal of

130 precipitation to various drip sites. This function is a lumped isotope model (named

131 ISODRIP) where precipitation enters the vadose zone trough a soil reservoir as well as

132 direct recharge by-passing the soil reservoir.

133

134 **2. Study site**

135 Our study site, Eagle Cave, is located in the south of Ávila province in central Spain

136 (40º9'15"N, 5º4'20"W). The cave is formed in a small hill 427 m above sea level that is

137 composed of dolomite and magnesite (Krklec et al., 2016). The cave has a main hall with

138 small passages beside, one of them serving as the entrance (Fig. 1A). The thickness of

139 bedrock over the cave is on average 16 m, being as thin as 8 m in some sectors over the

140 main hall and as thick as 22 m towards the edges of the hall and most lateral galleries

141   (Domínguez-Villar et al., 2013). A meteorological station operates outside Eagle Cave

142   since 2009, together with a system to collect accumulated precipitation samples at

143   monthly intervals for water stable isotope analyses (Krklec and Domínguez-Villar, 2014).

144   During the period 2009-2013 the mean annual temperature above the cave was 14.7 ºC,

145   the average amount of annual precipitation was 765 mm and the average annual potential

146   evapotranspiration (PET) according to Thornthwaite calculations (Thornthwaite, 1948) is

147   1163 mm. Freezing events in winter are short-lived and they do not freeze the soil (Krklec

148   et al., 2016). Snow and hail precipitation are rare at the studied site, so, rainwater is the

149   usual form of precipitation. Precipitation has a strong seasonality as expected from a

150   Mediterranean climate such as the one recorded at our study site, and PET is higher than

151   precipitation during 5 months per year: from May to September (Fig. 1B). The vegetation

152   above the cave consists of a typical Mediterranean forest with evergreen oaks and a dense

153   shrubs canopy. In the hill above the cave, rock exposures are common, although the red

154   soil, often up to 0.5 m thick, covers most of the hill surface over the carbonates (Krklec

155   et al., 2016).

156   Inside Eagle Cave, temperature and relative humidity are measured continuously

157   (Domínguez-Villar et al., 2013). Both temperature and relative humidity have a limited

158   natural seasonality, whereas these parameters exhibit even less variability as a result of

159   the impact of visitors to the cave (Domínguez-Villar et al., 2010). During the period 2009-

160   2013 the average cave temperature was 15.6 ±0.1 ºC (uncertainty accounts for 1 standard

161   deviation of daily data). Reliable relative humidity data has been acquired from 2011

162   onwards after installing a preheated probe (Vaisala HMP155), providing a relative

163   humidity of 99.2 ± 0.1 %. Water samples were collected in Eagle Cave at 11 drip sites

164   and 3 natural pools (See Table 1 in the supplementary material). In addition, water

165   samples were also collected from one location isolated from any drip where water was

166 left to equilibrate with cave atmosphere moisture. The selection of drip sites considered

167 a wide variety of drip rates and under the studied drip sites there are different types of

168 speleothems, from small candle-like speleothems to flowstones.

169

170 **3.- Methodology**

171 *3.1. Cave water sampling, drip rate monitoring and stable isotope analyses*

172 Cave water samples were collected during 5 years from 2008 until 2013 at uneven

173 intervals, ranging from less than 1 month to 4 months. Drip waters were collected in 30

174 ml HDPE bottles left under the drips with small plastic funnels to ensure that all drops

175 were collected (Fig. 1C). Depending on the drip rate, certain drip sites permitted

176 collecting samples within some minutes or hours, otherwise bottles were left under the

177 drips until a subsequent visit to the cave 1 to 3 weeks later. For this reason, two visits to

178 the cave were required during every sampling campaign. Even when discharge rates

179 allowed collecting samples within a day, often a bottle was left under those drips until the

180 subsequent visit within each sampling campaign to test any potential bias caused by the

181 sampling protocol. Pool water was collected with syringes. Water collected in the HDPE

182 bottles or with syringes was transferred to 2 ml glass vials and capped with lids having

183 septa. Whenever possible, vials were filled with water to the top taking special caution

184 that no airspace was left under the lid. Collected samples were stored under dark and cold

185 conditions in a fridge (i.e., around 4 ºC) until their analysis. One of the studied pools had

186 relatively constant water level, whereas in other two it varied. One of the pools with

187 variable water level drains completely during part of the year. At least one drip or water

188 flow is assumed to have provided water to the pools. The drainage of the pools is by

189 overflow and/or by seepage, and no evaporation is expected because of the high relative

190   humidity in the cave. Water collected from a cave pool was left to equilibrate with the

191   cave atmosphere moisture in a site with no drips. Several 30 ml bottles were used to

192   contain that water, and more than 6 months were left before the first water aliquot was

193   collected for its analysis. Since the cave atmosphere is saturated with water and air

194   currents are so slow that they were not appreciable during cave visits, these samples are

195   expected to follow the average isotope composition of the cave drips (Domínguez-Villar

196   et al., 2018). Small aliquots (i.e., 2 ml) of the equilibrated water were collected for

197   analysis during sampling campaigns.

198

199   Drip rate was measured at seven of the studied sites using Stalagmate drip counters

200   (Collister and Mattey, 2008). Not all drip sites were suitable to use drip counters (i.e.,

201   short distance to stalactite). In other cases, when several sites were located very close to

202   each other and show similar discharge, only one of the sites was equipped to optimize

203   resources. In drip sites without continuous monitoring, qualitative data on discharge

204   patterns was obtained based on field observations, including the amount of water

205   collected in every visit to the cave (Fig. 1D; Table 1 in supplementary material). Water

206   stable isotope analyses (δ^2H and δ^{18}O) were conducted at the University of Birmingham

207   using a Isoprime continuous-flow isotope ratio mass spectrometer. The water δ^2H

208   analyses were undertaken using the pyrolysis method over chromium in a Eurovector

209   elemental analyzer at 950 °C, while the δ^{18}O analyses were undertaken using an

210   equilibration technique in a Isoprime Multiflow. Raw analytical values were corrected for

211   instrumental drift and calibrated using both, internal laboratory standards UOB08 (δ^2H=-

212   40.40; δ^{18}O=-6.56), UOB09 (δ^2H=-157.60; δ^{18}O=-20.87) and UOB10 (δ^2H=-2.82;

213   δ^{18}O=-1.77) that have been calibrated to IAEA standards SLAP, V-SMOW and GISP.

214   All results are expressed using the δ-notation relative to the Vienna Standard Mean Ocean

215   Water (V-SMOW). The analytical uncertainty (internal precision) was typically <1.5‰

216   for δ^2H and <0.1 ‰ for $\delta^{18}O$ analyses. Whereas arithmetic isotope averages provide the

217   same weight to each isotope value in a series, weighted isotope averages balance each

218   isotope value by the amount of water contributed to the total amount of water in the

219   averaged series. Thus, weighted averages are calculated during mixing processes in this

220   paper to keep the mass balance of isotope compositions.

221   *3.2. Design of ISODRIP model*

222   We developed a new lumped model (e.g., Fairchild et al., 2006) that considers an

223   atmosphere layer, a soil layer and a vadose zone layer. A sketch of the model is provided

224   in figure 2. The model has a monthly resolution and required data are the monthly time

225   series of amount of precipitation, potential evapotranspiration and $\delta^{18}O$ composition of

226   precipitation, together with a series of soil and karst parameters, as well as the initial

227   values of water amount and its isotope composition in the different reservoirs considered

228   in the system (see Table 2 in the supplementary material). Although one of the time series

229   required is the potential evapotranspiration, the model calculates actual

230   evapotranspiration to have a realistic approach to soil water balance and the magnitude

231   and timing of large recharge events. All units of amount of water (volume) are reported

232   in mm to facilitate the comparison with precipitation, where the unit mm refers to mm/m^2

233   and that is equivalent to liters. The model is designed for the flow of water under low

234   environmental temperatures, since no water-rock isotope exchanges are considered. So,

235   the model might not be adequate to characterize the karst hydrology under hydrothermal

236   conditions.

237

238   Most of the precipitation infiltrates into the soil but a fraction of it is allowed to enter as

239   direct recharge to the epikarst (Fig. 2). Two components of direct recharge are enabled,

240   one that represents a constant proportion of precipitation (R_{d1}) to simulate bedrock

241   exposure at the surface, whereas the second component is a variable proportion depending

242   on the moisture conditions of the soil (R_{d2}) to simulate recharge through cracks or other

243   discontinuities in the soil. The total recharge that enters the vadose zone layer (R_T) flows

244   through the karst drainage system that may include interconnected conduits, fissures,

245   cracks, joints and pores. We have designed a vadose zone drainage system with four

246   different modules that account for different scenarios where particular flow regimes

247   dominate the seepage. Module A is characterized by diffuse flow under normal

248   environmental pressure conditions. Module B represents a diffuse flow drainage that is

249   subject to temporary overpressure conditions. This module simulates drip sites with large

250   variations in discharge rate but a well-mixed isotope signal. Overpressure conditions

251   occur when air in the diffuse flow network does not escape through the vadose zone and

252   soil during soil recharge events, increasing its atmospheric pressure that eventually

253   impacts the drip rate. Module C simulates a drip site that overflows from a storage within

254   the vadose zone that receives water from diffuse and preferential flow networks. The

255   secondary output of this module (drip C_2) is included only to keep the mass balance. The

256   discharge of drip C is continuous due to the diffuse flow component. Thus, although this

257   site never stops dripping, it has large variations in drip rate. Module D simulates the

258   underflow drainage of a storage within the vadose zone that receives water from diffuse

259   and preferential flow networks. The secondary output of this module (drip D_2) is only

260   included to keep the mass balance. This module is allowed to exhaust the storage and

261   provides a discontinuous record. The calculations made in module A are of key

262   importance to other modules, since all of them include at some point a diffuse component

263　in their flow. In module A, not all recharge water enters the diffuse flow network. There

264　is a threshold in the amount of water that can enter this network in every time step as a

265　result of its slow flow rate. Any recharge water that surpasses such threshold is deviated

266　to different modules as overflow water and enters the vadose zone in preferential flow

267　networks such as conduits or open fissures. When the recharge does not overpass the

268　maximum diffuse flow network threshold, most of the recharge enters the vadose zone as

269　diffuse flow, although a fraction of the recharge also enters conduits and open fissures. A

270　detailed description of the model and its mathematical expressions are provided in the

271　supplementary material.

272

273　The simulated isotope composition of different drips depends greatly on the parameters

274　selected to run the model. The initial selection of parameters requires the input of

275　estimated values by the operator, unless other sources of information are available (e.g.,

276　some parameters such as field capacity or percentage of rock exposure can be measured).

277　Obtaining the final selection of parameters involves a series of trial runs to find the best

278　fit between simulations and observations. During an initial evaluation of the selected

279　parameters, the amount of water in the different reservoirs of the model must reproduce

280　the cave hydrology observations (e.g., drips have continuous or discontinuous flow). A

281　proper evaluation of the hydrological balances of the flow networks or storages considers

282　not only the seasonality but also the inter-annual variability. The next criteria to select the

283　model parameters is the amplitude of isotope variability of the drip waters. To complete

284　the trial runs, the absolute value of drip water isotope composition and its long-term

285　variability are adjusted to select the final model parameters. Since many parameters have

286　a limited range of variability capable to reproduce observations (e.g., to keep a steady

287　state of inter-annual amount of water in the system), simulations are substantially

288 constrained by observations, reducing the impact of the selected parameters by the

289 operator.

290

291 **4. Results**

292 *4.1. Eagle Cave water isotope record*

293 The stable isotope composition (δ^{18}O and δ^2H) of 300 cave water samples was analyzed

294 for this study. Samples were collected during 26 sampling campaigns each of them

295 consisting of two visits to the cave. The high relative humidity measured in the cave (i.e.,

296 >98%) is consistent with negligible evaporation processes within the cave, which is

297 supported by the lack of enrichment in oxygen-18 of samples exposed to cave atmosphere

298 during sampling campaigns (Fig. 3A). Most cave waters have a constrained range of

299 isotope values and δ^{18}O-δ^2H relationship. However, we identified a limited number of

300 cave water samples (N=13) that provided anomalous results when compared to the rest

301 of the record within each sampling sites (see text section 1.2 in the supplementary

302 material). Those anomalous samples were not removed from the database or the graphs

303 but were not used in calculations. We compare the isotope composition of cave waters to

304 the local meteoric water line (Fig. 3A). The isotope variability along the local meteoric

305 water line is used to split the cave water sites in two groups: sites with well-mixed waters

306 and sites with partially-mixed waters. The partially-mixed cave waters nicely follow the

307 local meteoric water line, whereas the well-mixed cave waters have a limited variability,

308 although all samples sit on top of the local meteoric water line. So, the isotope signature

309 of the collected cave waters does not record any measurable sign of evaporation in the

310 cave, the vadose zone or the soil.

311

312　The δ^{18}O records show that most cave waters of all sites have an isotope composition that

313　falls within the range of variability of the annually weighted average δ^{18}O values of

314　precipitation, that during the studied period was 1.83‰ (Fig. 3B). No seasonal δ^{18}O

315　variability is observed in the partially-mixed or the well-mixed cave waters despite the

316　obvious seasonality in the precipitation δ^{18}O record (Fig. 3C). The monthly δ^{18}O

317　variability of precipitation is ~10‰, whereas the partially-mixed cave waters show a

318　variability of ~3‰ and the well-mixed waters have a variability ~1‰. Most of the

319　variability recorded in the well-mixed cave waters corresponds to long-term isotope

320　changes. The long-term trend of the δ^{18}O record of well-mixed cave waters does not

321　follow a simple smooth and/or delayed signal of the precipitation δ^{18}O record. However,

322　the good fit of the cave waters isotope signature to the local meteoric water line and its

323　annually weighted isotope composition of precipitation supports the view that water

324　originates from precipitation. Nevertheless, the δ^{18}O variability of cave waters depends

325　on complex admixtures of precipitation within the karst system that transform the original

326　signal.

327

328　*4.2. Simulation of the soil water and recharge*

329　Actual evapotranspiration was calculated considering the amount of water available in

330　the soil and the potential evapotranspiration. The results of the calculated actual

331　evapotranspiration show that the hydrological deficit is restricted to four months per year

332　(i.e., May to August), and that ~40% of precipitation is either stored in the soil or enters

333　the vadose zone as recharge, whereas ~60 % of the precipitation is returned to the

334　atmosphere as actual evapotranspiration (Fig. 4A). Because of the direct recharge

335　components, the vadose zone receives recharge every month in which there is

precipitation. During the 2009-2013 period, the direct recharge accounted for ~32% of recharge into the vadose zone (Fig. 4B). Thus, most of the recharge occurs when accumulated water in the soil exceeds the field capacity, a component of recharge that in the model is labeled as R_S. The contribution of the R_S component to the total recharge is discontinuous, with only 30% of the months during the studied period having R_S recharge. A clear R_S seasonal pattern is observed during years with abundant precipitation recorded during the rainy season, although during dry years the contribution of R_S is limited and lacks a clear seasonality. Water infiltrated in the soil is accumulated in this reservoir until it is removed by evapotranspiration or is flushed to the vadose zone as recharge. Thus, precipitation that is infiltrated every month in the soil mixes with the water that was already accumulated in that reservoir. The mixing of water in the soil reduces the amplitude of precipitation $\delta^{18}O$ values (i.e., ~10‰) and provides a series of modelled monthly soil water with $\delta^{18}O$ values that varied ~3‰ (Fig. 4C).

During periods when there is Rs, the total recharge can be up to one order of magnitude larger than during periods when all recharge originates from direct recharge components. Most of the water that enters the aquifer when R_S is the prevailing source of recharge goes to preferential flows. Therefore, during large recharge events, only a limited percentage enters the diffuse flow network and contributes to the isotope composition of well-mixed drip waters.

4.3. Simulation of well-mixed cave waters

ISODRIP model considers four different modules within the vadose zone layer. The modules A and B capture the signal of well-mixed cave waters, being A the general case, and B a specific situation that could affect certain drips. Results of the module A show

360   that the amount of water stored in the diffuse flow network of the aquifer above the

361   simulated drip site (A_{DfA}) has a stable long-term signal and a limited intra-annual

362   variability regarding seasonal or inter-annual amount of recharge (Fig. 5A). The

363   discharge of water in the simulated drip site of module A (Q_A) is small and has limited

364   variability, nicely simulating the characteristics of slow and continuous drip sites (Fig.

365   5B). During recharge events, only a limited amount of water enters the diffusional flow

366   network of Module A (R_{TDf}), whereas any volume of water above the selected threshold

367   is diverted to preferential flows (R_{TPf}). The simulation suggests that the contribution of

368   total recharge to the diffuse flow network (R_{TDf}) is <25% (Fig. 5B), whereas the rest of

369   the recharge is diverted by preferential flows (R_{TPf}). In the diffuse flow network, direct

370   recharge contributions are more frequent than recharge events from soil water, but the

371   latter reach the maximum capacity of recharge that this network can assimilate in every

372   event. Thus, the contribution to total recharge that enters the diffuse flow drainage

373   network is equally distributed (~50%) between direct recharge (R_d) and soil water

374   recharge (R_S). These results support that the direct recharge has a major role in controlling

375   the hydrology of the diffuse flow system and cannot be ignored.

376

377   The module A of ISODRIP simulates the isotope composition of water at the top of the

378   diffuse flow network in the vadose zone (δ_{DfA}) that accounts for the mixing of recharge

379   and underground water. The residence time [transit time] of water in [through] the diffuse

380   flow network is given by the ratio between the accumulated water in the network and the

381   discharge. According to ISODRIP, the residence time of water in the diffuse flow network

382   of Eagle Cave is on average 15 months. Once this parameter is known the isotope

383   composition of the network at the top of the aquifer is mixed and transferred to the

384   simulated drip site. Thus, the $\delta^{18}O$ composition of the simulated drip in module A (δ_A) is

385   a smoothed and delayed signal of the water at the top of the diffuse flow network in the

386   vadose zone (δ_{DfA}). In Eagle Cave, the simulated drip water isotope composition lacks

387   any seasonality, as expected from the estimated residence time, although the larger

388   changes in $\delta^{18}O$ still can occur within less than a year.

389

390   Some of the monitored drip sites have well-mixed waters according to their isotope

391   signature, although they also have highly variable drip rates. The well-mixed isotope

392   composition of the drip waters supports that the source of water is from the diffuse flow

393   network. However, the fast discharge rates recorded in some sites would exhaust the

394   limited capacity of the water network in module A. However, for these cases we have

395   developed the particular case of module B, that allows lateral flow within the diffuse flow

396   network. In this module, enhanced drip rates are not the results of preferential flow, but

397   overpressure conditions in the diffuse flow network during recharge events that prevents

398   the flow of air in the network to be equilibrated with atmospheric pressure at the surface.

399   The simulation supports changes of drip rate larger than one order of magnitude without

400   exhausting the water in the diffuse flow network (Fig. 5C). However, since this drainage

401   module allows lateral flow and creates temporal hydrological depression cones, it is

402   obvious that this module cannot be a dominant drip site system without affecting the

403   general pattern of surrounding drip sites. In Eagle Cave, the module B drainage system

404   was only assigned to three drips clustered in a small chamber, whereas all other drips

405   associated to diffusional flow were characterized by the module A drainage system.

406

407   The faster discharge rate enables more water to enter the diffuse network during large

408   recharge events. Since such recharge events often have more negative $\delta^{18}O$ values, the

409   isotope composition of the water at the top of the diffuse flow network in the vadose zone

410   (δ_{DfB}) and the isotope composition of the drip water (δ_B) have a slight bias towards more

411   negative $\delta^{18}O$ values (Fig. 5D). The maximum $\delta^{18}O$ differences between the simulated

412   drip A and drip B (~0.3‰) occurred after 2010, a year that was unusually wet and had

413   more negative $\delta^{18}O$ values of precipitation. Aside from slight biases in the $\delta^{18}O$ signal,

414   both modules follow a similar structure during the modelled period.

415

416   *4.4. Simulation of partially-mixed cave waters*

417   To simulate the $\delta^{18}O$ signal of partially-mixed cave water, ISODRIP incorporates two

418   modules (C and D) that represent preferential flow drainages that pass through different

419   storages were preferential and diffuse water drainages interact. Module C represents the

420   overflow of a storage that results in a drip with continuous flow. Module D represents the

421   underflow of a storage that results in a drip with discontinuous flow. The designed

422   hydrological network has secondary outflow routes in each module (drip C2 and drip D2).

423   These outflow drainages are essential to enable hydrological stability to the main module

424   drips replicating the observed dynamics in Eagle Cave, although they are not the focus of

425   the simulation in the module.

426   The discharge of the main drip of module C captures the overflow drainage of a storage

427   (SC) that accumulates water from preferential and diffusional flows. Discharge of this

428   drip (Q_C) has a high flow rate when preferential water overflows the storage, while

429   records a limited drip rate otherwise. The transition between flow rates is sharp (Fig 6A).

430   However, the amount of water in the storage (A_{SC}) is relatively stable, with sharp

431   increases when preferential flow operates and gradual decreases otherwise due to the

432   diffuse outflow drainage. The $\delta^{18}O$ composition of the storage (δ_{SC}) and the drip (δ_C) have

433   a range of 2.5‰ with more negative values when preferential flows trigger higher drip

434   rates, and $\delta^{18}O$ values more similar to those in the module A when diffuse flow drainage

435   dominate the discharge (Fig. 6B). The model captures nicely the magnitude of the isotopic

436   anomalies and the timing of some of them, but fails to predict every single isotope

437   negative anomaly. This hydrological design does not simulate isotope anomalies less

438   negative than those simulated by modules A and B, and consequently does not reproduce

439   the full set of partially-mixed $\delta^{18}O$ values recorded.

440

441   The discharge of the main drip of module D (Q_D) captures the drainage of a storage (S_D)

442   that accumulates water from preferential and diffusional flow drainages. In this case, S_D

443   has an underflow that enables the complete drain out of the storage sometime after the

444   preferential flow drainage ceased. In this module, the discharge of the main drip of the

445   module (Q_D) provides more gradual transitions after the flow through preferential

446   drainages ceases and the drip stops once the storage drains out completely. The simulated

447   discharge reproduces the discontinuous drip pattern observed in several drips in Eagle

448   Cave (Fig. 6C). The $\delta^{18}O$ composition of the storage (δ_{SD}) and the drip (δ_D) have a range

449   of 3‰ (Fig. 6D). The simulation is a discontinuous time series that sometimes shares

450   variability with the well-mixed cave water $\delta^{18}O$ signal but also has important anomalies

451   around it. Most of the anomalies provide more negative $\delta^{18}O$ excursions, although this

452   module also simulates less negative $\delta^{18}O$ anomalies in relation to well-mixed cave water

453    $\delta^{18}O$ signal. Although δ_D covers most of the range of isotope variability recorded in Eagle

454   Cave, the timing of events is difficult to replicate accurately.

455

456   *4.5. Comparison of observed and simulated cave water $\delta^{18}O$ records*

457   Sampling sites were characterized according to their hydrological and isotope variability

458   to different modules of ISODRIP (see Table 1 in supplementary material). The simulated

459     $\delta^{18}O$ signals of drips A, B, C and D were compared with the observed $\delta^{18}O$ data of those

460   sites represented within each module. Simulations of drip sites C and D were compared

461   with measured waters from all sites that had partially-mixed $\delta^{18}O$ records, regardless if

462   they were characterized as overflow or underflow drainages. The module A, that

463   simulates a drip characterized by a diffuse flow drainage, is represented in the cave by

464   seven of the monitored sites. The simulated $\delta^{18}O$ signal of drip A has the highest

465   correlation when compared to the $\delta^{18}O$ observations (r = 0.82; p-value <0.005) and

466   explains 68% of the variance of the $\delta^{18}O$ observations (Fig. 7). The range between the

467   confidence intervals of the regression overlaps with the uncertainty of observations in all

468   samples except one, although in this case, only two sites were available to characterize

469   the variability of all cave waters during that month. However, this regression has

470   discarded three months (N=25) that were clear outliers. A justification for the removal of

471   these outliers is provided in the supplementary material. Module B also characterizes

472   diffusional flow drainages, although in this case, overpressure conditions during recharge

473   events enable highly variable drip rates. Three of the monitored drip sites, all of them

474   located in the cave within one square meter, were characterized under this drainage

475   regime (Fig. 1C). The correlation coefficient between the simulated drip B $\delta^{18}O$ signal

476   and the observed $\delta^{18}O$ record is also high (r = 0.76, p-value <0.005) and explains 58% of

477   the variance of observed data (Fig. 7). All observations considering their uncertainties

478   overlap with the range between the confidence intervals of the regression, although from

479   17 observations two were clear outliers and were removed from the analysis.

480

481   Module C, that represents an overflow storage drainage, has the lowest correlation

482   between simulated and observed δ^{18}O data (r = 0.56, p-value <0.005) and explains 31%

483   of the variance of δ^{18}O observations (N=26) (Fig. 7). All sites with partially-mixed δ^{18}O

484   signal were used for the comparison (5 sites; see Table 2 in the supplementary material).

485   However, it is not clear that any of the studied drip sites will be dominated by this kind

486   of flow regime. No data were removed from the dataset despite an outlier is recorded,

487   since no clear justification was found to discard the values of that month. Module D, that

488   represents an underflow storage drainage, has an unexpectedly high correlation

489   coefficient between simulated and observed δ^{18}O data (r = 0.73, p-value <0.005) and

490   explains 54% of the variance of the observations (Fig. 7). However, it has to be kept in

491   mind that the simulation considers a discontinuous record and that the period of flow of

492   different observed sites not always coincides with the simulated drip site, limiting the

493   number of observations (N=15). Although the simulated and observed δ^{18}O values do not

494   record outliers, when considering the uncertainties of observations two data points do not

495   fit within the range between the confidence intervals of the regression.

496

497   **5. Discussion**

498   *5.1. Implementation of ISODRIP model to Eagle Cave*

499   The hydrological results of ISODRIP model capture the structure of the main drips

500   monitored in Eagle Cave as well as reproduce the mean value and variability of the δ^{18}O

501   record. The simulation suggests that the mean residence time of the diffuse flow in the

502   main chamber of the cave is on average 15 months and captures very well the inter-annual

503   δ^{18}O variability, including the exceptionally more negative δ^{18}O values of precipitation

504   during the year 2010. However, the simulated δ^{18}O signal provides a slightly smoother

505   signal than the observations. The simulations of modules A and B assume a pure

506   diffusional flow, whereas the real hydrology of the system is likely to be more complex.

507   Thus, although many of the studied sites are dominated by diffuse flow drainages, this

508   does not prevent the existence of secondary sources from preferential flows that could

509   interact at any point during the transit time with the diffuse flow network, increasing its

510   δ^{18}O variability.

511

512   Models with preferential flow drainage are more complex to evaluate. Five sites recorded

513   cave water with partially-mixed δ^{18}O values suggesting that those sites were dominated

514   by preferential flow regimes. We designed module C to provide a continuous flow and

515   module D to produce a discontinuous flow. The monitoring of three drips showed that

516   after each wet season, when all the sites suddenly increase their discharge, they

517   progressively decrease their drip rate until eventually dry out. This gradual decrease of

518   discharge suggests an underflow drainage (module D). However, since there is no

519   evaporation in the cave, hydrologically there is no clear way to determine if the pool water

520   is sourced predominantly from overflow (module C) or underflow drips (module D). The

521   simulations of preferential flows show that values less negative than the δ^{18}O signal

522   simulated with modules A and B are only possible when implementing the module D (not

523   the module C). Since all monitored sites that record partially-mixed waters have in their

524   time series δ^{18}O values less negative than the simulations of modules A and B, the model

525   supports that all studied sites having significant preferential flows are better characterized

526   by module D: an underflow drainage regime (Fig. 8). Since the cave has thousands of drip

527   sites, is likely that many of them would be dominated by overflow drainage regimes, but

528   none of the 15 sites that we selected for this study provided signals compatible with that

529   regime. The correlation of the observed $\delta^{18}O$ record of sites with partially-mixed waters

530   and the simulated $\delta^{18}O$ signals of the modelled drip site D is relatively high. However,

531   since the simulated drip D provides a discontinuous record that not always coincides with

532   the periods of discharge in the different monitored sites, the overall time series (Fig. 6D)

533   suggests that the good fit of the simulation and observations might be overestimated.

534

535   The calculated actual evapotranspiration suggests that during the studied period ~60% of

536   the precipitation returned to the atmosphere by evaporation or transpiration. This

537   distinction is important, because evaporation is a process that results in kinetic

538   fractionation whereas transpiration does not (Gat, 2010). Therefore, although we do not

539   record evaporation in the cave, it is obvious that a significant fraction of water was

540   evaporated while stored in the soil, before recharge events flushed it into the epikarst to

541   participate into every drip water in the cave. However, the isotope signature of water

542   collected in Eagle Cave does not record any sign of significant evaporation in relation to

543   the local meteoric water line. The lack of evaporative signature in the isotope signal is

544   common to cave waters from regions with very different climates. To reproduce realistic

545   cave water $\delta^{18}O$ signals, models often use unrealistically low fractionation factors

546   (Wackerbarth et al., 2010; Treble et al., 2013), whereas other simply ignore the

547   evaporation processes in the soil (Partin et al., 2012; Moerman et al., 2014; Domínguez-

548   Villar et al., 2018; Jean-Baptiste et al., 2019). ISODRIP model follows the latter approach

549   regarding isotope fractionation in the soil. Although the remaining soil water fraction

550   would have higher $\delta^{18}O$ values, major precipitation events responsible for triggering

551   recharge have often relatively low $\delta^{18}O$ values, minimizing the impact of evaporation in

552   soil water (Dansgaard, 1964; Gat, 1996; Lachniet et al., 2009). In addition, dew produced

553   from condensation of atmospheric moisture (Aravena et al., 1989) or even dew originated

554   from soil water moisture (Kaseke et al., 2017) likely counteract part of the evaporative

555      $\delta^{18}O$ biases. Therefore, it is not unusual that shallow underground water would be used

556   as a good approximation to the long-term weighted isotope composition of precipitation,

557   as is the case in Spain (Plata, 1994).

558

559   Water left to equilibrate with the moisture of the cave atmosphere has a $\delta^{18}O$ signal that

560   follows the well-mixed cave waters. Since drainage through the diffuse flow network

561   better reproduces the isotope observations, the recorded $\delta^{18}O$ variability in equilibrated

562   water samples suggests that diffuse flow networks provide most of the moisture to the

563   cave atmosphere. However, the reality is slightly more complex. The implementation of

564   ISODRIP in Eagle Cave supports that >75% of recharge flows through the preferential

565   flow network characterized by having partially-mixed $\delta^{18}O$ signals. However, not even

566   during large events of recharge the $\delta^{18}O$ signal of the cave atmosphere is significantly

567   affected, as recorded by the water samples equilibrated with the atmosphere. The site

568   where equilibrated samples were collected is far from major preferential flow drainages

569   (e.g., major flowstones), although the advection in the main hall tends to homogenize the

570   atmosphere (Domínguez-Villar et al., 2013) limiting any local impact. The $\delta^{18}O$ values

571   of cave waters that deviate from the well-mixed isotope signature are short-lived and the

572   timing of enhanced discharge that goes along with such deviations differs greatly

573   depending on flow routes. Therefore, waters with partially-mixed $\delta^{18}O$ signals smooth

574   their anomalies into the dominant $\delta^{18}O$ signal (i.e., well-mixed cave waters). In Eagle

575   Cave, the water equilibrated with the cave atmosphere is impacted by both, diffuse and

576   preferential flow drainages, although individual drip anomalies are smoothed resulting in

577 a well-mixed $\delta^{18}O$ signal comparable to the one recorded by drainages of the diffuse flow

578 network (Fig. 3C). Similar observations were reported in a different cave where

579 evaporation in the studied chamber is also negligible (Domínguez-Villar et al., 2018).

580

581 *5.2. Implications of ISODRIP model to paleoclimate research*

582 During the last decade, drip water isotope modelling has shown that in caves without

583 evaporation recorded in the cave water $\delta^{18}O$ signal, different drips can result in very

584 different signals despite having the same input parameters (e.g., Baker et al., 2012). For

585 this reason, replication of speleothems is essential to evaluate which speleothem $\delta^{18}O$

586 anomalies can be attributed to changes in the climate/environment and which $\delta^{18}O$

587 anomalies fall in the natural range of $\delta^{18}O$ variability within a cave caused from different

588 flow routes in the vadose zone (e.g., Jex et al., 2013; Hercman et al., 2020). Speleothem

589 paleoclimate researchers often assume that outside the tropics, the speleothem $\delta^{18}O$

590 records, as well as the vadose zone water, have $\delta^{18}O$ compositions biased towards winter

591 (e.g., Pape et al., 2010; Moreno et al., 2014), because of the limited recharge during

592 summer months due to enhanced evapotranspiration and in some cases also the limited

593 precipitation. This could justify a theoretical correlation between speleothems and winter

594 climate indexes (Baldini et al., 2008; Deininger et al., 2016), although speleothem records

595 from Europe do not support the assumption of a strong recharge bias towards winter

596 (Mischel et al., 2015). On the other hand, in tropical regions, drip water $\delta^{18}O$ signal of

597 some caves has been suggested to be biased towards the summer monsoon season,

598 because this is when most of the recharge takes place (Partin et al., 2012; Breitenbach,

599 2015). However, drip water often records mean drip $\delta^{18}O$ values very close to the

600 weighted isotope composition of the precipitation (Moerman et al., 2014; Duan et al.,

601   2016). Therefore, observations do not support a systematic bias of drip water $\delta^{18}O$ signal,

602   in comparison with the mean weighted isotope composition of precipitation, towards the

603   season with larger recharge.

604

605   Some cave water $\delta^{18}O$ models assume direct flow of precipitation into the aquifer (Partin

606   et al., 2012; Genty et al., 2014; Moerman et al., 2014; Mischel et al., 2015; Jean-Baptiste

607   et al., 2019). However, soil is an efficient filter that controls recharge and greatly impacts

608   the recharge $\delta^{18}O$ composition (Comas-Bru et al., 2015). So, more sophisticated $\delta^{18}O$

609   hydrological models include a soil layer (e.g., Wackerbarth et al., 2010; Treble et al.,

610   2013; Domínguez-Villar et al., 2018). ISODRIP is the first cave water $\delta^{18}O$ model to

611   account for direct recharge components as well as having a soil layer. This innovation

612   enables every single month with precipitation to account for the cave water $\delta^{18}O$

613   composition regardless of the existence of seasonality in the major recharge events.

614   Including a direct recharge component is a more realistic approach for many karst

615   aquifers, since rock exposures are common in karst landscapes. This feature of the model

616   is particularly important when applied to Mediterranean and semiarid/arid environments.

617   Under these climates, soil cover is often discontinuous and rock exposures represent large

618   percentages of land surface, allowing a fraction of precipitation to enter the vadose zone

619   without passing through the soil filter. So, for sites where direct recharge takes place, all

620   significant precipitation events affect the cave water $\delta^{18}O$ composition independently of

621   the month in which they occur.

622

623   There is another hydrological phenomenon that limits the impact of large seasonal

624   recharge events biasing the average drip $\delta^{18}O$ signals in relation to the mean weighted

625     $\delta^{18}O$ composition of precipitation. Soil recharge events often involve larger volume of

626   water that cannot be assimilated at once by the diffuse flow drainage network. So, during

627   large recharge events, most of the recharge is transferred underground by preferential

628   flow networks (i.e., conduits and fissures). So, only drips dominated by preferential flow

629   drainages will record certain $\delta^{18}O$ bias towards periods of recharge, whereas those drips

630   dominated by diffuse flow would have a minimal impact. A maximum threshold for the

631   amount of recharge entering the diffuse flow network was already implemented in

632   previous cave water $\delta^{18}O$ models (e.g., Jean-Baptiste et al., 2019) and this feature is also

633   included in ISODRIP. Thus, the impact of direct recharge and the maximum threshold of

634   the aquifer to assimilate recharge water, explain the good fit of many cave water $\delta^{18}O$

635   values with the annually weighted average $\delta^{18}O$ values of precipitation in caves from

636   different climates (Goede et al., 1982; Yonge et al., 1985; Caballero et al., 1996;

637   Fleitmann et al, 2004; Lambert and Aharon, 2010). Considering the processes described

638   above, we do not support the idea that climate over the cave controls a systematic bias of

639   drip water $\delta^{18}O$ values in relation to mean weighted $\delta^{18}O$ values of precipitation (Baker

640   et al., 2019). Instead, drip sites dominated by preferential flow routes as well as drip sites

641   with evaporative processes within the vadose zone are likely to be behind most

642   divergences.

643

644   Cave water studies have demonstrated that understanding the role of evaporation in cave

645   waters is critical to properly interpret the variability of speleothem $\delta^{18}O$ records (Cuthbert

646   et al., 2014; Feng et al., 2014). In addition, cave water $\delta^{18}O$ models have demonstrated

647   that for the same cave, multiple drip $\delta^{18}O$ signals with a wide compositional range can be

648   the result of different flow routes (Fig. 8). The $\delta^{18}O$ variability related to different flow

649 routes may be larger than the amplitude expected for large climate anomalies such as

650 Younger Dryas (Baker et al., 2013). Thus, instead of doing general assumptions, to

651 properly understand a speleothem $\delta^{18}O$ record, it is critical to characterize the hydrology

652 of the drip site that formed the studied speleothem, as well as its relationship with the

653 mean weighted $\delta^{18}O$ signal of precipitation. Nevertheless, particular drips might have

654 non-stationary dynamics (Moerman et al., 2014), and not in all cases the monitoring

655 results could be extrapolated to the past. Sometimes there is no certainty in linking

656 speleothems and specific drip sites or is obvious that the drip dynamics have changed

657 through time (e.g., changes in flow route due to micro-collapses within the vadose zone

658 or filling of fissures/porosity by detrital/chemical deposits). In these cases, replication of

659 various speleothem records covering the same time period is recommended to evaluate

660 the variability of $\delta^{18}O$ in the cave/chamber (e.g., Domínguez-Villar et al., 2017; Hercman

661 et al., 2020). The replication of multiple speleothem records is time and resource

662 consuming, but provides a reliable signal and narrows down the impact of hydrology in

663 the composite $\delta^{18}O$ record variability. Replication studies are important independently of

664 the goal of the speleothem research being on meteorological events such as hurricanes or

665 cyclones (e.g., Partin et al., 2012) or on long-term climate changes. Most replication test

666 are typically designed to constrain the impact of kinetic fractionation (Dorale and Liu,

667 2009) and frequently only two speleothems are compared (e.g., Wang et al., 2001).

668 However, to characterize the variability of paleo drip water $\delta^{18}O$ signature in a

669 cave/chamber based on speleothem $\delta^{18}O$ records, replications based on more than two

670 speleothems are desirable. In any case, $\delta^{18}O$ models of drip waters suggest that to prevent

671 misinterpreting anomalies in speleothem $\delta^{18}O$ records, replication should become a

672 common practice in paleoclimate studies not just to evaluate kinetic effects, but also to

673 understand the internal variability introduced in the signal by the karst hydrology.

674

6. Conclusions

We have developed a new cave water isotope hydrological model (ISODRIP) that captures not only the mean $\delta^{18}O$ composition of observed drip water and its variability, but also reproduces nicely the inter-annual variability of the signal. ISODRIP considers four different flow scenarios to capture diffuse and preferential flow drainages in the system. Module A characterizes drips with diffuse flow under atmospheric pressure conditions. Drips with limited drip rate variability and a well-mixed drip water $\delta^{18}O$ signals should be simulated with this module. Module B characterizes drips with diffuse flow under temporal overpressure conditions. Drip sites with large drip rate variations and well-mixed drip water $\delta^{18}O$ signals should be simulated with this module. Module C represents drips with diffusional and preferential flows passing through an overflow storage. Drip sites with a continuous and very variable discharge that record partially-mixed $\delta^{18}O$ signals should be simulated with this module. Finally, module D represents drips where diffuse and preferential flows circulate through a underflow storage. Drip sites with a discontinuous record and partially-mixed $\delta^{18}O$ signals should be simulated with this module. Each module can be adjusted to reproduce as many virtual drip sites as desired. The simulations include a direct recharge component in the soil layer that enables precipitation from any significant event to contribute to the cave water oxygen isotope composition. Therefore, we provide evidence to support that recharge is unlikely to be limited to certain periods of the year (e.g., winter), including in Mediterranean, semiarid or even arid climates unless in specific drip sites dominated by preferential flows. The best fit of our simulated and observed $\delta^{18}O$ signals is for diffuse flow drainages. In these cases, the simulations suggest that in Eagle Cave the average residence time of water in

the vadose zone above the cave is 15 months. The relative humidity in Eagle Cave is always nearly 100% and consequently no evaporation is recorded in the cave water $\delta^{18}O$ record in relationship to the local meteoric water line. Water exposed to the moisture of the cave atmosphere records a well-mixed $\delta^{18}O$ signal similar to water from diffuse flow drainages, since the anomalies introduced by the preferential flow drainages are not synchronous and are progressively smoothed.

We described the conditions for diffuse flow drainages to be capable to provide well-mixed $\delta^{18}O$ signals even when discharge rates increase exponentially as a response to recharge events. The module that simulates such conditions enables a temporary lateral water flow component for particular drip sites where pressure builds up in the drainage network during recharge events. Simulation of preferential flow drainages is more complex to reproduce, although the magnitude of $\delta^{18}O$ events was properly captured. The monthly timescale of the model is likely insufficient to simulate accurately the flow through preferential conduits and its interaction with different storage components, although provides a good approximation to the average $\delta^{18}O$ composition of cave waters and its variability.

Acknowledgements

722 thank the suggestion of four anonymous reviewers that improved the original version of

723 this manuscript.

724

725 REFERENCES

726 Aravena, R., Suzuki, O., Pollastri, A., 1989. Coastal fog and its relation to groundwater

727   in the IV region of northern Chile. Chemical Geology 79, 83-91.

728 Arbel, Y., Greenbaum, N., Lange, J., Inbar, M., 2010. Infiltration processes and flow rates

729   in developed karst vadose zone tracers in cave drips. Earth Surface Processes and

730   Landforms 35, 1682-1693.

731 Ayalon, A., Bar-Matthews, M., Sass, E., 1998. Rainfall-recharge relationships within a

732   karstic terrain in the Eastern Mediterranean semi-arid region, Israel: $\delta^{18}O$ and δD

733   characteristics. Journal of Hydrology 207, 18–31.

734 Baker, A., Bradley, C., 2010. Modern stalagmite $\delta^{18}O$: instrumental calibration and

735   forward modelling. Global and Planetary Change 71, 201–206.

736 Baker, A., Bradley, C., Phillips, S.J., 2013. Hydrological modeling of stalagmite $\delta^{18}O$

737   response to glacial-interglacial transitions. Geophysical Research Letters 40, 3207–

738   3212.

739 Baker A., Bradley, C., Phillips, S.J., Fischer, M., Fairchild, I.J., Fuller, L., Spötl, C.,

740   Azcurra, C., 2012. Millennial-length forward models and pseudoproxies of

741   stalagmite $\delta^{18}O$: an example from NW Scotland. Climate of the Past 8, 1153-1167.

742 Baker, A., Fairchild, I.J., 2012. Drip water hydrology and speleothems. Nature Education

743   Knowledge 3(10), 16.

744   Baker, A., Hartmann, A., Duan, W., Hankin, S., Comas-Bru, L., Cuthbert, M.O., Treble,

745   P.C., Banner, J., Genty, D., Baldini, L.M., Bartolomé, M., Moreno, A., Pérez-Mejías,

746   C., Werner, M., 2019. Global analysis reveals climatic controls on the oxygen isotope

747   composition of cave drip water. Nature Communications 10, 2984.

748   Baldini, L.M., McDermott, F., Foley, A.M., Baldini, J.U.L., 2008. Spatial variability in

749   the European winter precipitation δ^{18}O-NAO relationship: implications for

750   reconstructing NAO-mode climate variability in the Holocene. Geophysical

751   Research Letters 35, L04709.

752   Bar-Matthews, M., Ayalon, A., Matthews, A., Sass, E., Halicz, L., 1996. Carbon and

753   oxygen isotope study of active water-carbonate system in a karstic Mediterranean

754   cave: implications for paleoclimate research in semiarid regions. Geochimica et

755   Cosmochimica Acta 60, 337-347.

756   Bradley, C. Baker, A., Jex, C.N., Leng, M.J., 2010. Hydrological uncertainties in the

757   modelling of cave drip-water δ^{18}O and the implications for stalagmite paleoclimate

758   reconstructions. Quaternary Science Reviews 29, 2201-2214.

759   Breitenbach, S.F.M, Lechleitner, F.A., Meyer, H., Diengdoh, G., Mattey, D., Marwan,

760   N., 2015. Cave ventilation and rainfall signals in dripwater in a monsoonal setting- a

761   monitoring study from NE India. Chemical Geology 402, 111-124.

762   Caballero, E., Jiménez de Cisneros, C., Reyes, E. 1996. Applied Geochemistry 11, 583-

763   587.

764   Carrasco, F., Andreo, B., Liñán, C., Mudry, J., 2006. Contribution of stable isotopes to

765   the understanding of the unsaturated zone of a carbonate aquifer (Nerja Cave,

766   southern Spain). Comptes Rendus Geoscience 338, 1203-1212.

767 Chapman, J.B., Ingraham, N.L., Hess, J.W., 1992. Isotopic investigation of infiltration

768   and unsaturated zone flow processes at Carlsbad Cavern, New Mexico. Journal of

769   Hydrology 133, 343-363.

770 Collister, C., Mattey, D., 2008. Controls on water drop volume at speleothem drip sites:

771   An experimental study. Journal of Hydrology 358, 259-267.

772 Comas-Bru, L., McDermott, F., 2015. Data-model comparison of soil-water δ^{18}O at a

773   temperate site in N. Spain with implications for interpreting speleothem $\delta1^8$O.

774   Journal of Hydrology 530, 216–224.

775 Cuthbert, M.O., Rau, G.C., Andersen, M.S., Roshan, H., Rutlidge, H., Marjo, C.E.,

776   Markowska, M., Jex, C.N., Graham, P.W., Mariethoz, G., Acworth, R.I., Baker, A.,

777   2014. Evaporative cooling on speleothem drip water. Scientific Reports 4, 5162.

778 Dansgaard, W., 1964. Stable isotopes in precipitation. Tellus 16, 436–468.

779 Deininger, M., Werner, M., McDermott, F., 2016. North Atlantic oscillation controls on

780   oxygen and hydrogen isotope gradients in winter precipitation across Europe;

781   implications for paleoclimate research. Climate of the Past 12, 2127-2143.

782 Domínguez-Villar, D., Fairchild, I.J., Baker, A., Carrasco, R.M., Pedraza, J., 2013.

783   Reconstruction of cave temperature based on surface atmosphere temperature and

784   vegetation changes: implications of speleothem palaeoclimate records. Earth and

785   Planetary Science Letters 369–370, 158–168.

786 Domínguez-Villar, D., Fairchild, I.J., Carrasco, R.M., Pedraza, J., Baker, A., 2010. The

787   effect of visitors in a touristic cave and the resulting constraints on natural thermal

788   conditions for palaeoclimate studies (Eagle Cave, Central Spain). Acta Carsologica

789   39, 491-502.

790   Domínguez-Villar, D., Krklec, K., López-Sáez, J.A., Sierro, F.J., 2020. Thermal impact

791   of Heinrich stadials in cave temperature and speleothem oxygen isotope records.

792   Quaternary Research 1-14, doi:10.1017/qua.2020.99.

793   Domínguez-Villar, D., Lojen, S., Krklec, K., Baker, A., Fairchild, I.J., 2015. Is global

794   warming affecting cave temperatures? Experimental and model data from a

795   paradigmatic case study. Climate Dynamics 54, 569–581.

796   Domínguez-Villar, D., Lojen, S., Krklec, K., Kozdon, R., Edwards, R.L., Cheng, H.,

797   2018. Ion microprobe $\delta^{18}O$ analyses to calibrate slow growth rate speleothem records

798   with regional δ^{18} records of precipitation. Earth and Planetary Science Letters 482,

799   367–376.

800   Domínguez-Villar, D., Wang, X., Krklec, K., Cheng, H., Edwards, R.L., 2017. The

801   control of the tropical North Atlantic on Holocene millennial climate oscillations.

802   Geology 45, 303-306.

803   Dorale, J.A., Liu, Z., 2009. Limitations of Hendy test criteria in judging the paleoclimatic

804   suitability of speleothems and the need for replication. Journal of Cave and Karst

805   Studies 71, 73-80.

806   Duan, W., Ruan, J., Luo, W., Li, T., Tian, L., Zeng, G., Zhang, D., Bai, Y., Li, J., Tao,

807   T., Zhang, P., Baler, A., Tan, M., 2016. The transfer of seasonal isotopic variability

808   between precipitation and drip water at eight caves in the monsoon regions of China.

809   Geochimica et Cosmochimica Acta 183, 250-266.

810   Even, H., Carmi, I., Magaritz, M., Gerson, R., 1986. Timing the transport of water through

811   the upper vadose zone in a karstic system above a cave in Israel. Earth Surface

812   Processes and Landforms 11, 181-191.

813   Fairchild, I.J., Baker, A., 2012. Speleothem Science: From Process to Past Environments.

814   John Wiley-Blackwell, Oxford.

815   Fairchild, I.J., Tuckwell, G.W., Baker, A., Tooth, A.F., 2006. Modelling of dripwater

816   hydrology and hydrochemistry in a weakly karstified aquifer (Bath, UK):

817   Implications for climate change studies. Journal of Hydrology 321, 213-231.

818   Feng, W., Casteel, R.C., Banner, J.L., Heinze-Fry, A., 2014. Oxygen isotope variations

819   in rainfall, drip-water and speleothem calcite from a well-ventilated cave in Texas,

820   USA: Assessing a new speleothem temperature proxy. Geochimica et Cosmochimica

821   Acta 127, 233-250.

822   Fitts, C.R., 2012. Growndwater Science (2nd edition). Academic Press, Elsevier,

823   Waltham, MA, 696 pp.

824   Fleitmann, D., Burns, S.J., Neff, U., Mudelsee, M., Mangini, A., Matter, A., 2004.

825   Palaeoclimatic interpretation of high-resolution oxygen isotope profiles derived from

826   annually laminated speleothems from Southern Oman. Quaternary Science Reviews

827   23, 935-945.

828   Fuller, L., Baker, A., Fairchild, I.J., Spötl, C., Marca-Bell, A., Dennis, P.F., 2008. Isotope

829   hydrology of dripwaters in a Scottish cave and implications for stalagmite

830   paleoclimate research. Hydrology and Earth System Sciences 12, 1065-1074.

831   Gat, J.R., 1996. Oxygen and hydrogen isotopes in the hydrological cycle. Annual Review

832   of Earth and Planetary Sciences 24, 225–262.

833   Gat, J.R., 2010. Isotope Hydrology: A Study of the Water Cycle. Imperial College

834   Press, London.

835 Gehrels, J.C., Peeters, J.E.M., de Vries, J.J., Dekkers, M., 1998. The mechanism of soil
836   water movements as inferred from 18O stable isotope studies. Hydrological Sciences
837   Journal 43, 579-594.

838 Genty, D., Labuhn, I., Hoffmann, G., Danis, P.A., Meste, O., Bourges, F., Wainer, K.,
839   Massault, M., Van Exter, S., Régnier, E., Orengo, P., Falourd, S., Minster, B.,
840   2014. Rainfall and cave water isotope relationships in two South-France sites.
841   Geochimica et Cosmochimica Acta 131, 323–343.

842 Goede, A., Green, D.C., Harmon, R.S., 1982. Isotopic composition of precipitation, cave
843   drips and actively forming speleothems at three Tasmanian cave sites. Helictite 20,
844   17-27.

845 Hercman, H., Gąsiorowski, M., Pawlak, J., Błaszczyk, M., Gradiński, M., Matoušková,
846   S., Zawidzki, P., Bella, P., 2020. Atmospheric circulation and the differentiation of
847   precipitation sources during the Holocene inferred from five stalagmite records from
848   Demänová Cave System (Central Europe). The Holocene 30, 834-846.

849 Jean-Baptiste, P., Genty, D., Fourré, E., Régnier, E., 2019. Tritium dating of dripwater
850   from Villars Cave (SW-France). Applied Geochemistry 107, 152-158.

851 Jex, C.N., Phillips, S.J., Baker, A., Bradley, C., 2013. Reducing uncertainty in the
852   climatic interpretations of speleothem δ^{18}O. Geophysical Research Letters 40,
853   2259–2264.

854 Kaseke, K.F., Wang, L., Seely, M.K., 2017. Nonrainfall water origins and formation
855   mechanisms. Science Advances 3, e1603131.

856   Kaufman, A., Bar-Matthews, M., Ayalon, A., Carmi, I., 2003. The vadose flow above

857   Soreq Cave, Israel: a tritium study of the cave waters. Journal of Hydrology 273,

858   155-163.

859   Kluge, T., Riechelmann, D.F.C., Wieser, M., Spötl, C., Sültenfuß, J., Schröder-Ritzrau,

860   A., Niggemann, S., Aeschbach-Hertig, W., 2010. Dating cave drip water by tritium.

861   Journal of Hydrology 394, 396–406.

862   Krklec, K., Domínguez-Villar, D., 2014. Quantification of the impact of moisture

863   source regions on the oxygen isotope composition of precipitation over Eagle Cave,

864   central Spain. Geochimica et Cosmochimica Acta 134, 39–54.

865   Krklec, K., Domínguez-Villar, D., Carrasco, R.M., Pedraza, J., 2016. Current

866   denudation rates in dolostone karst from central Spain: Implications for the

867   formation of unroofed caves. Geomorphology 264, 1-11.

868   Lachniet, M.S., 2009. Climatic and environmental controls on speleothem oxygen-

869   isotope values. Quaternary Science Reviews 28, 412-432.

870   Lambert, W.J., Aharon, P., 2010. Oxygen and hydrogen isotopes of rainfall and dripwater

871   at DeSoto Caverns (Alabama, USA): Key to understanding past variability of

872   moisture transport from the Gulf of Mexico. Geochimica et Cosmochimica Acta 74,

873   846-861.

874   Liñán, C., del Rosal, Y., Carrasco, F., Vadillo, I., Benavente, J., Ojeda, L., 2018.

875   Highlighting the importance of transitional ventillation regimes in the management

876   of Mediterranean show caves (Nerja-Pintada system, southern Spain). Science of the

877   Total Environment 631-632, 1268-1278.

878   Markowska, M., Baker, A., Andersen, M.S., Jex, C.N., Cuthbert, M.O., Rau, G.C., Gra-

879   ham, P.W., Rutlidge, H., Mariethoz, G., Marjo, C.E., Treble, P.C., Edwards, N.,

880   2016. Semi-arid zone caves: evaporation and hydrological controls on δ^{18}O drip

881   water composition and implications for speleothem paleoclimate reconstructions.

882   Quaternary Science Reviews 131, 285–301.

883   Mischel, S.A., Scholz, D., Spötl, C., 2015. δ^{18}O values of cave drip water: a promising

884   proxy for the reconstruction of the North Atlantic Oscillation? Climate Dynamics

885   45, 3035.

886   Moerman, J.W., Cobb, K.M., Partin, J.W., Meckler, A.N., Carolin, S.A., Adkins, J.F.,

887   Lejau, S., Malang, J., Clark, B, Tuen, A.A., 2014. Transformation of ENSO-related

888   rainwater to dripwater δ^{18}O variability by vadose water mixing. Geophysical

889   Research Letters 41, 7907-7915.

890   Moore, G.W., Sullivan, G.N., 1978. Speleology: the Study of Caves. Zephyrus Press,

891   Teaneck, NJ (USA).

892   Moreno, A., Sancho, C., Bartolomé, M., Oliva-Urcia, B., Delgado-Huertas, A., Estrela,

893   M.J., Corell, D., López-Moreno, J.I., Cacho, I., 2014. Climate controls on rainfall

894   isotopes and their effects on cave drip water and speleothem growth: the case of

895   Molinos cave (Teruel, NE Spain). Climate Dynamics 43, 221–241.

896   Pape, J.R., Banner, J.L., Mack, L.E., Musgrove, M., Guilfoyle, A., 2010. Controls on

897   oxygen isotope variability in precipitation and cave drip waters, central Texas, USA.

898   Journal of Hydrology 385, 203-215.

899   Partin, J.W., Jenson, J.W., Banner, J.L., Quinn, T.M., Taylor, F.W., Sinclair, D., Hardt,

900   B., Lander, M.A., Bell, T., Miklavič, B., Jocson, J.M.U., Taboroši, D., 2012.

901   Relationship between modern rainfall variability, cave dripwater, and stalagmite

902   geochemistry in Guam, USA. Geochemistry, Geophysics, Geosystems 13, Q03013.

903   Pérez-Mejías, C., Moreno, A., Sancho, C., Bartolomé, M., Stoll, H., Osácar, C., Cacho,

904   I., Delgado-Huertas, A., 2018. Geochimica et Cosmochimica Acta 243, 66-98.

905   Pflitsch, A., Wiles, M., Horrocks, R., Piasecki, J., Ringeis, J., 2010. Dynamic

906   climatologic processes of barometric cave systems using the example of Jewel Cave

907   and Wind Cave in South Dakota, USA. Acta Carsologica 39, 449-462.

908   Plata, A., 1994. Composición isotópica de las precipitaciones y aguas subterráneas de la

909   Península Ibérica. CEDEX, Madrid.

910   Thornthwaite, C.W., 1948. An approach toward a rational classification of climate.

911   Geographical Review 38, 55-94.

912   Treble, P.C., Bradley, C., Wood, A., Baker, A., Jex, C.N., Fairchild, I.J., Gagan, M.K.,

913   Cowley, J., Azcurra, C., 2013. An isotopic modelling study of flow paths and

914   storage in Quaternary calcarenite, SW Australia: implications for speleothem

915   paleoclimate records. Quaternary Science Reviews 64, 90-103.

916   Villar, E., Fernandez, P.L., Quindós, L.S., Solana, J.R., Soto, J., 1983. Temperature of

917   rock surface in Altamira Cave (Spain). Transactions of the British Cave Research

918   Association 10, 165-170.

919   Wackerbarth, A., Scholz, D., Mangini, A., 2010. Modelling the $\delta^{18}O$ value of cave drip

920   water and speleothem calcite. Earth and Planetary Science Letters 299, 387-397.

921   Wang, Y.D., Cheng, H., Edwards, R.L., An, Z.S., Wu, J.Y., Shen, C.C., Dorale, J.A.,

922   2001. A high-resolution absolute-dated Late Pleistocene monsoon record from Hulu

923   Cave, China. Science 294, 2345-2348.

924 Yamada, M., Ohsawa, S., Matsuoka, H., Watanabe, Y., Brahmantyo, B., Maryunani,

925 K.A., Tagami, T., Kitaoka, K., Takemura, K., Yoden, S., 2008. Derivation of travel

926 time of limestone cave drip water using tritium/helium 3 dating method. Geophysical

927 Research Letters, 35, L08405.

928 Yonge, C.J., Ford, D.C., Gray, J., Schwarcz, H.P., 1985. Stable isotope studies of cave

929 seepage water. Chemical Geology 58, 97-105.

930

932
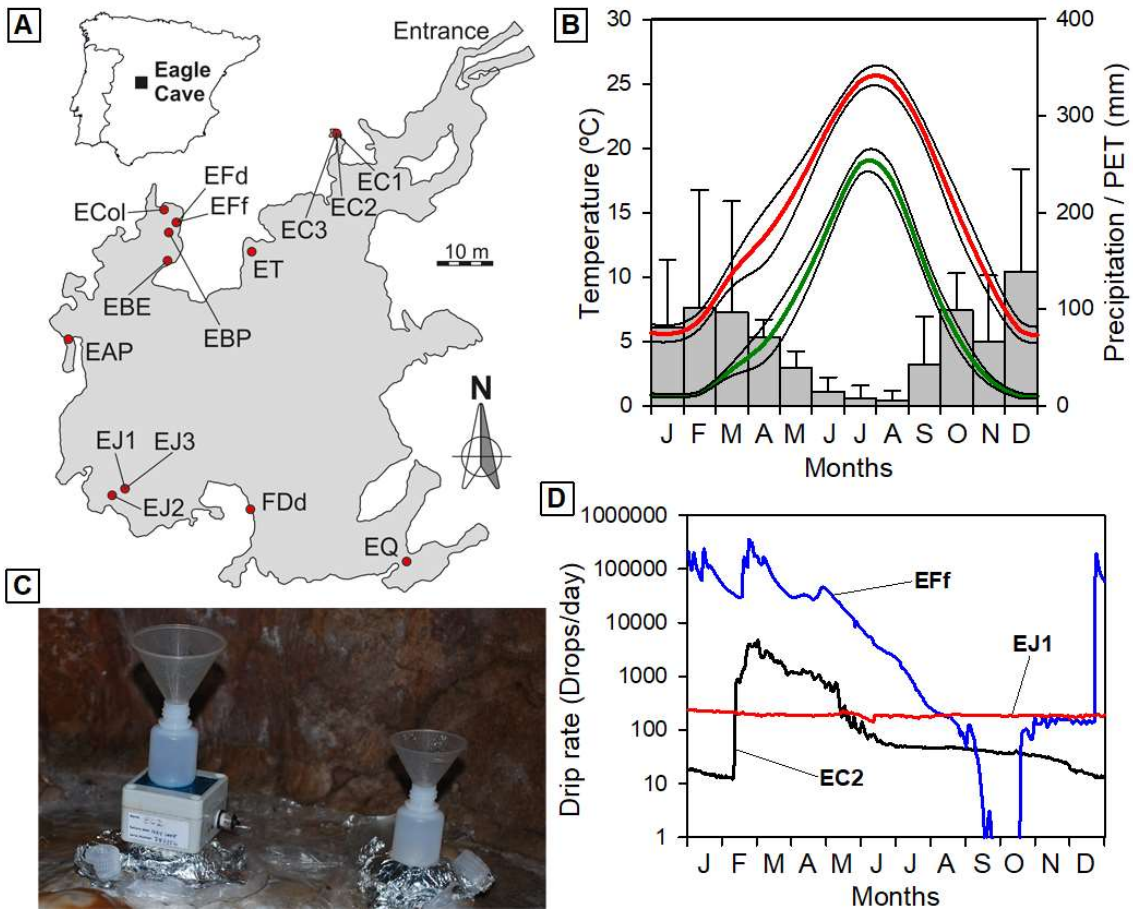
934 Fig. 1. Eagle Cave settings and sampling sites. A) Sketch of Eagle Cave showing the

935 location of sampling sites. The inset map (top left) shows the cave location within the

936 Iberian Peninsula. B) Climate diagram of the studied site for the years 2009 to 2013,

937 including potential evapotranspiration. Curve in red represents temperature, in green is

938 for PET and grey bars are for precipitation. C) Drip sites EC1 (left) and EC2 (right) during

939 a water collection campaign. D) Examples of annual drip rate records from 3 drip sites

940 with different flow regimes. EFf: highly variable drip rate and discontinuous flow, EJ1:

941 limited drip rate and continuous flow, EC2: bi-modal drip rate and continuous flow.

942

943

944
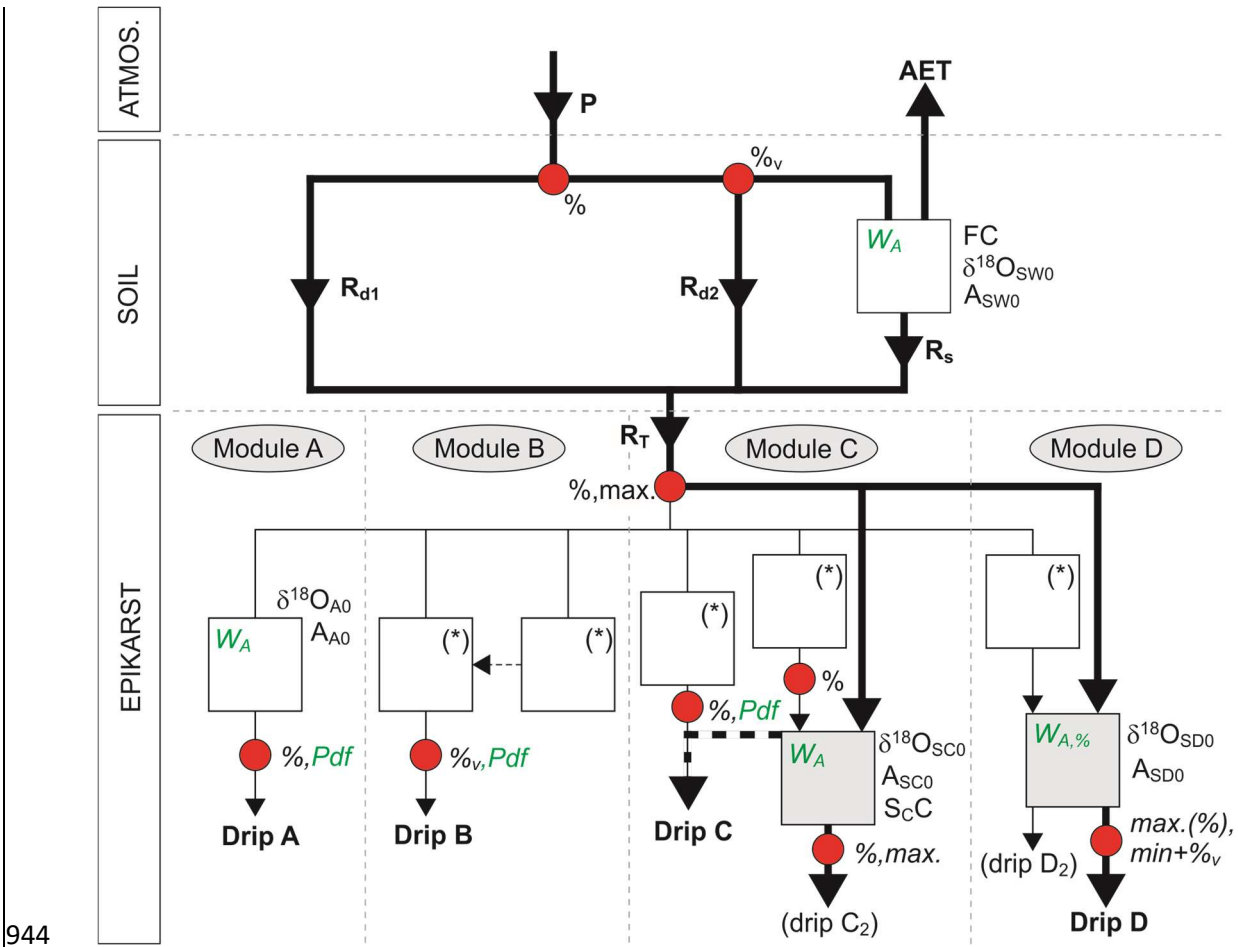
Fig. 2. Sketch of ISODRIP model to simulate the isotope composition of vadose zonewaters. The model has three layers, atmosphere, soil and vadose zone and four modules to represent different hydrological scenarios in the vadose zone layer. Module A is for diffuse drainage under atmospheric pressure, module B for diffuse flow under temporal overpressure conditions, module C is for drainages with preferential and diffusional flows circulating through an overflow storage that results in continuous discharge and module D for drainages with preferential and diffuse flows circulating through an underflow storage that results in discontinuous discharge. The output of the model provides the amount of water and the isotope composition of different drips in a hypothetical cave. Lines and arrows indicate the flow of water in the system as

preferential flow drainage (thick lines) or diffuse flow drainage (thin lines). Discontinuous lines represent conditional flow. Rectangles represent water reservoirs, they have a white filling when the reservoir is a network across the full layer (i.e., soil interconnected porosity and vadose zone diffuse flow network) or are filled in grey color when they represent storages (i.e., large open fissures or other cavities) within the vadose zone. The isotope composition of water in every reservoir is averaged considering the amount of water from each contributing source. W_A: Isotope values weighted by the amount of water from every contributing source, including the reservoir itself. Red dots are nodes where the flow is controlled by at least one operation. All operation symbols are in italics, colored in green when describing just a function, or in black when the function requires entering an input parameter to be defined by the user. $W_{A,\%}$: Isotope values calculated using a percentage for every source of water in addition to their amount of water contributed. The black % symbol indicates that a percentage of water can flow in a certain direction, the rest being directed in a different direction or continues being accumulated in the preceding reservoir. $\%_v$: indicates that the percentage of flow is variable. Pdf is a probability distribution function. max. and min.: are maximum or minimum thresholds of flow; max. (%): a maximum percentage of flow is considered. Drip A, B, C and D are the main drips simulated, although the model also includes two subsidiary outflows or drips (i.e., drip C_2 and D_2) that are only introduced to keep the mass balance. Initial amount of water (A_0) and isotope composition (δ_0) of different reservoirs are required input parameters. These reservoirs are indicated by the subscripts: SW for the water accumulated in the soil, A for water in the diffuse flow network, SC and SD for water in the storages from module C and D, respectively. Other variables are also reported in this sketch. P stands for precipitation, AET is the actual evapotranspiration; R_{d1} and R_{d2} are two components of direct recharge, R_T is the total recharge and FC the

980   field capacity. In module C, the storage that collects preferential flows has a maximum

981   capacity (CS_C) controlled by the position of the overflow conduit. The symbol (*) in

982   epikarst reservoirs indicates that the initial parameters and average weighting in these

983   reservoirs is identical to the reservoir in the module A.

984

985

986
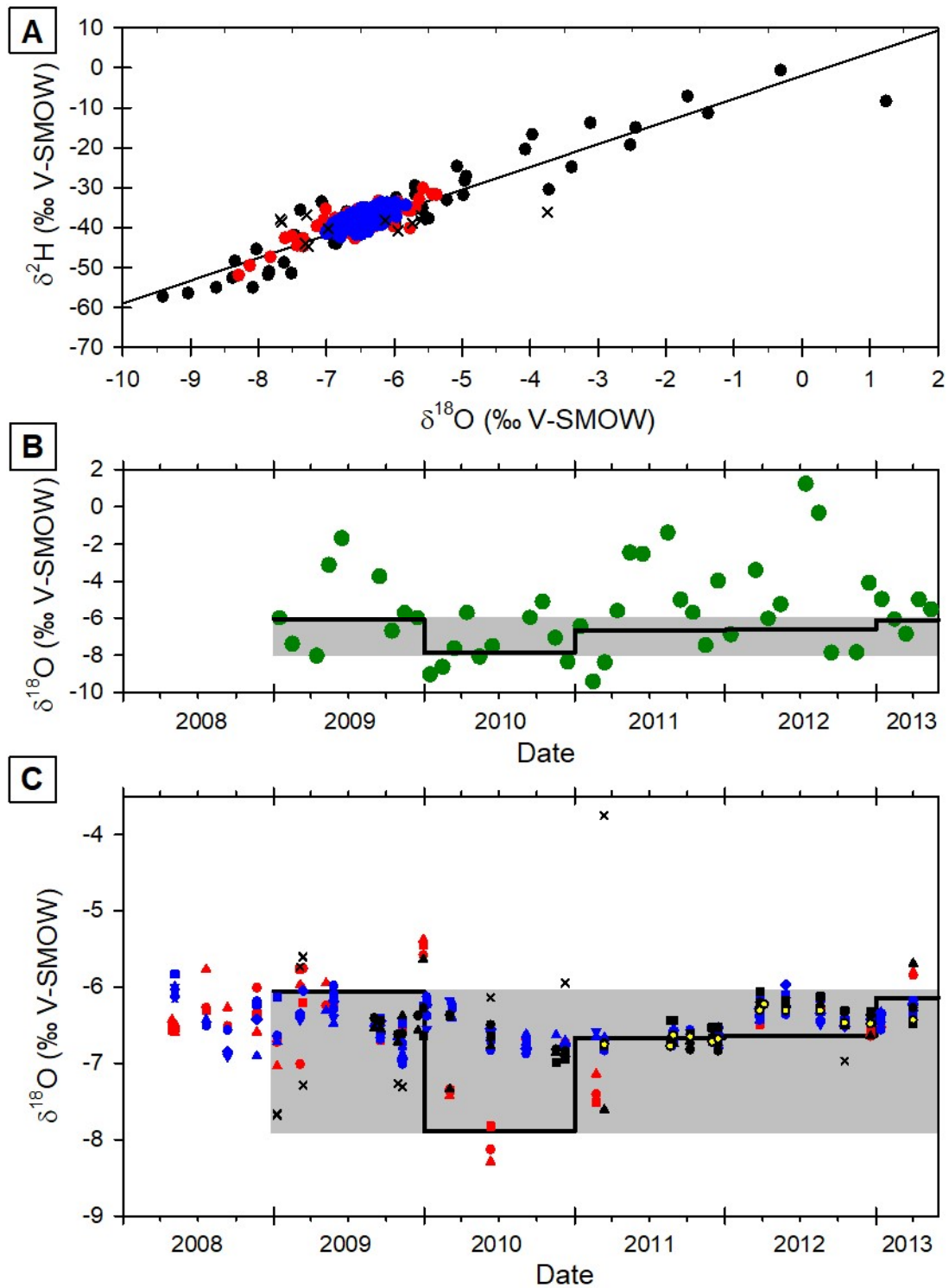
Fig. 3. Isotope records at the studied site. A) Graph showing the δ^2H and $\delta^{18}O$ relationship

of precipitation and cave waters. Black dots: monthly rainwater samples. Red dots:

989 partially-mixed cave waters. Blue dots: well-mixed cave waters. Crosses: anomalous

990 analyses. Cave waters overlie the local meteoric water line with no signs of deviation due

991 to evaporation. B) Monthly precipitation $\delta^{18}O$ record (green dots) at the meteorological

992 station outside Eagle Cave. The black line shows the annually weighted $\delta^{18}O$ record of

993 precipitation ($\delta^{18}O_{pw}$). The grey rectangle shows the range of variability of $\delta^{18}O_{pw}$. C)

994 Cave water $\delta^{18}O$ record. The black line and grey rectangle are the $\delta^{18}O_{pw}$ record as in the

995 panel B. Red symbols: drip sites with partially-mixed waters (triangle: ECol, circle: Eff,

996 square: EFd). Blue symbols: drip sites with well-mixed waters (star: EBE, triangle: ET,

997 circle: EJ1, square: EJ3, diamond: EJ2, hexagon: EC1, inverted triangle: EC2, vertical

998 stripe: EC3). Black symbols: Pool waters (triangle: EBP, circle: EAP, square: FdD),

999 Yellow circles: water equilibrated with the cave atmosphere. Crosses: anomalous

1000 analyses.

1001
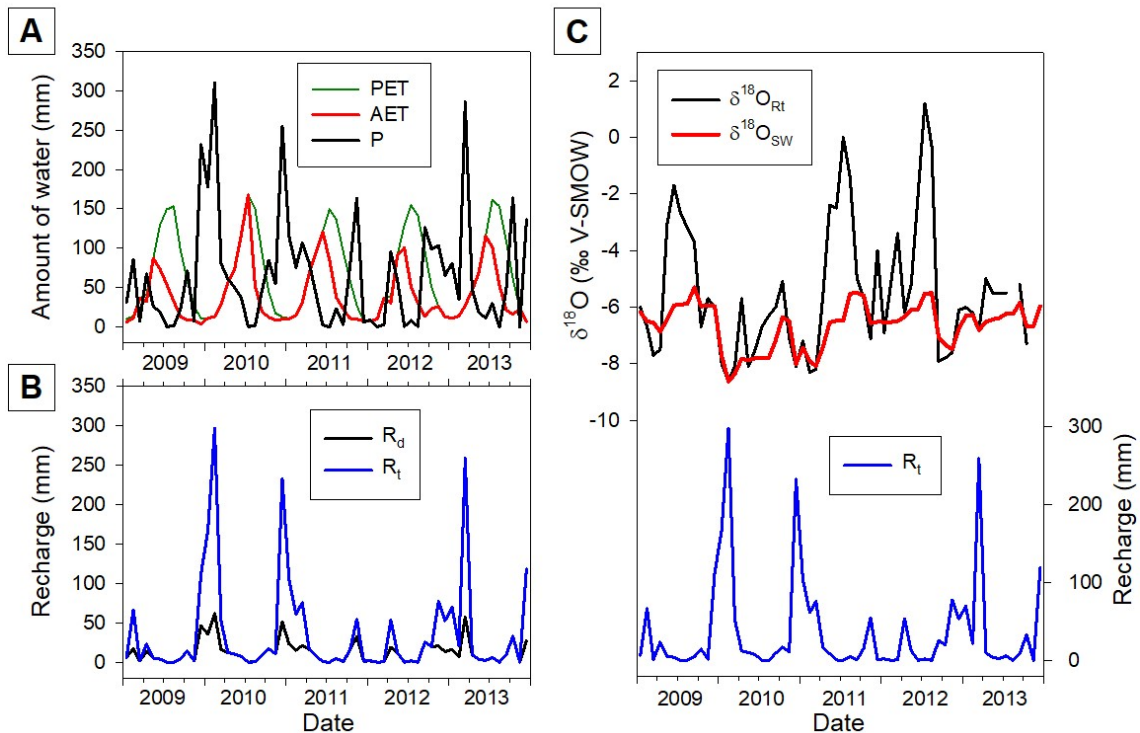
1003

1004   Fig. 4. Simulation of time series of the soil water components and their isotope

1005   composition above Eagle Cave during the period 2009-2013. A) Graph showing the

1006   relationship among precipitation (P), potential evapotranspiration (PET) and actual

1007   evapotranspiration (AET). B) Main contributions to recharge. The direct recharge (R_d)

1008   represents the sum of the two direct recharge components considered in ISODRIP, R_{d1}

1009   and R_{d2}. Total recharge (R_T) is the sum of soil recharge (R_S) and direct recharge (R_d)

1010   components. C) Isotope composition of water stored in the soil (red curve) and total

1011   recharge water (black curve). The lower panel shows the amount of recharge every month.

1012   Outstanding positive/less negative isotope anomalies of water from the R_d source

1013   contributes to the recharge with small but significant amount of water. Large peaks of R_T

1014   (blue curve) occur during different periods of the year and during those periods, the

1015   isotope variability range of R_T (black curve) is < 2‰.
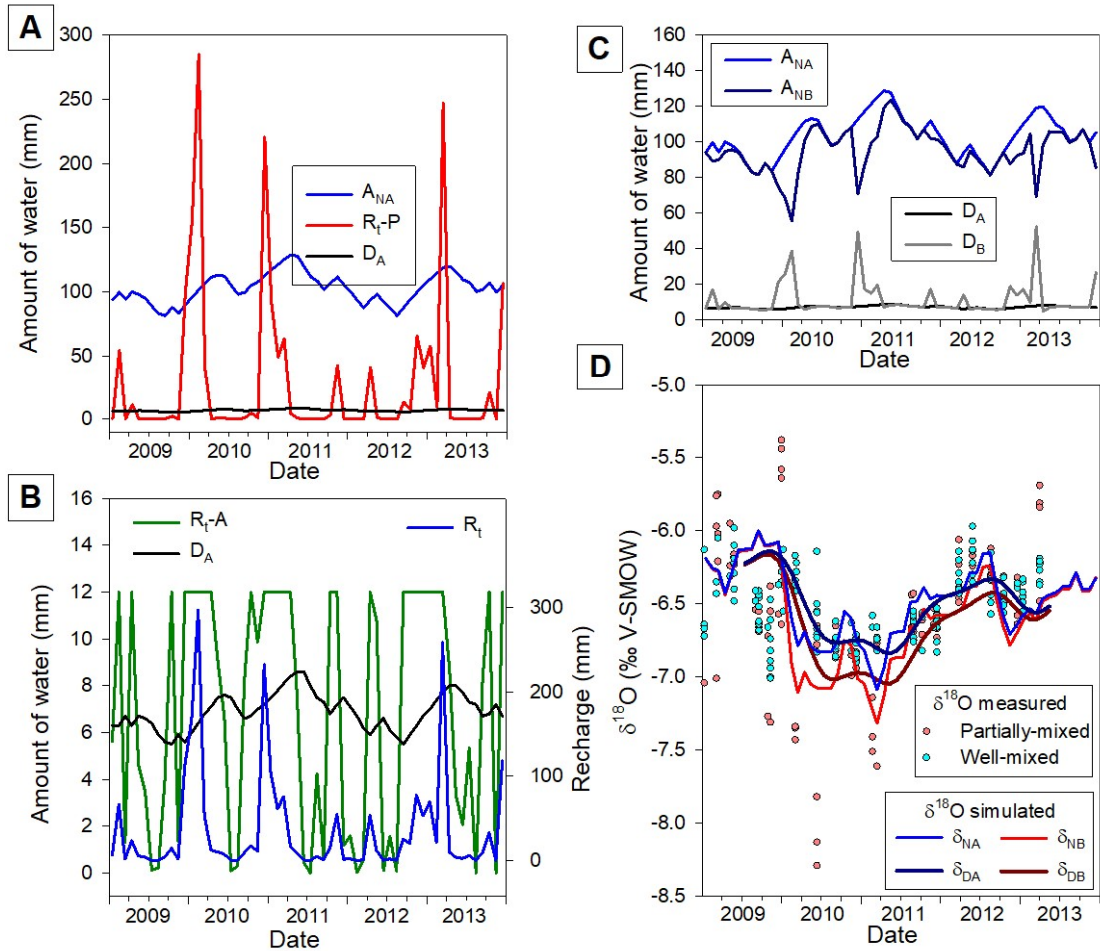
Fig. 5. Simulation of diffuse flow drainage in modules A and B. A) Main hydrological components of module A simulation. A_{DfA}: amount of water accumulated in the diffuse flow network of module A, R_{TPf}: amount of total recharge diverted to preferential flows, Q_A: discharge at drip site A. B) Details of the hydrological response of module A. R_T: total recharge, R_{TDf}: amount of total recharge that enters the diffuse flow network. The right axis is scale only for R_T. C) Main hydrological components of modules A and B.

1025   Amount of water accumulated in the diffusional flow network of modules A and B (A_{DfA}

1026   and A_{DfB}). Discharge at drip sites A and B (Q_A and Q_B). D) Simulated $\delta^{18}O$ signal of

1027   water from the upper section of the aquifer according to modules A and B (δ_{DfA} and δ_{DfB})

1028   and at the drip sites A and B (δ_A and δ_B). Observed $\delta^{18}O$ data are also plotted for
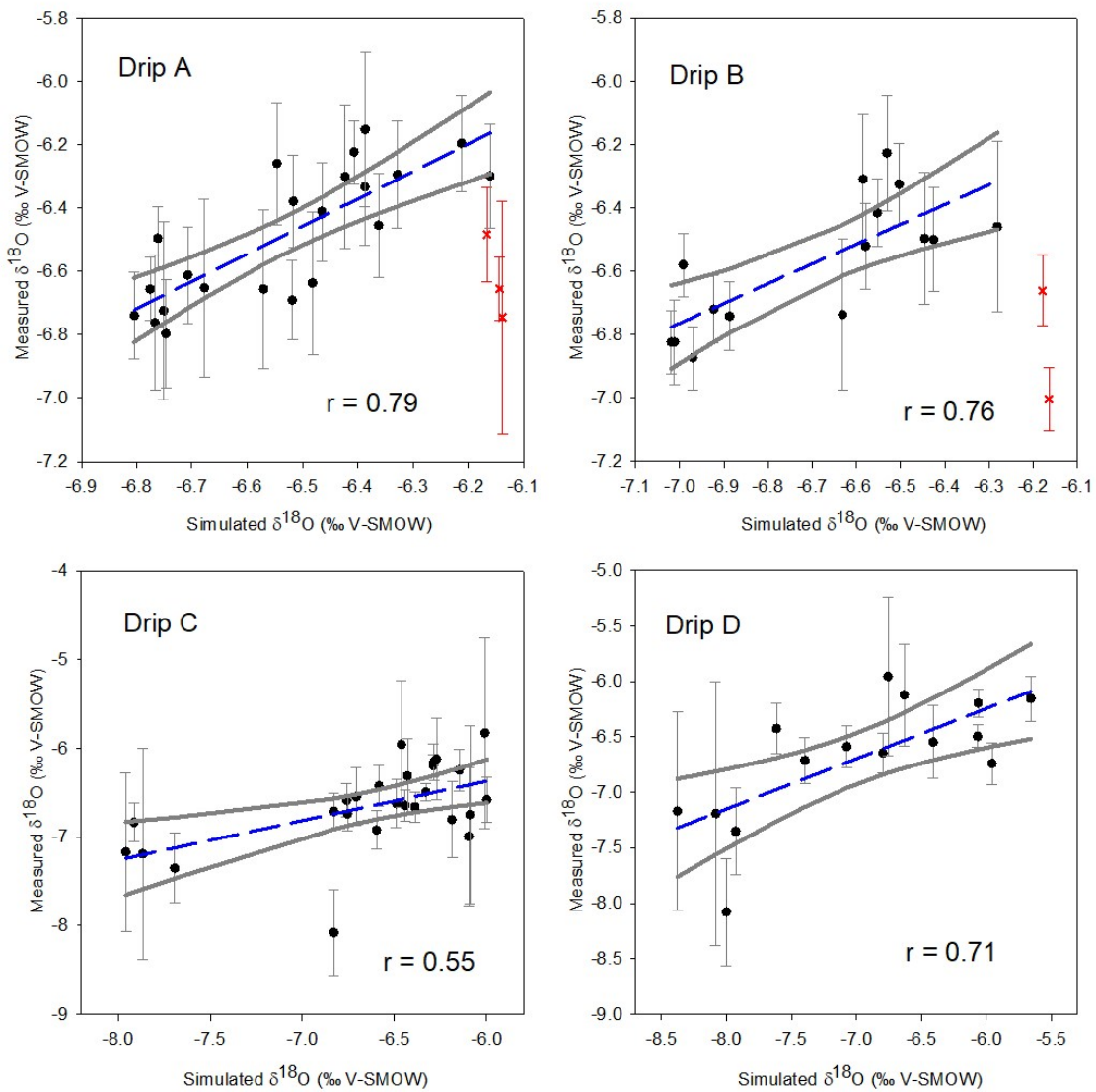
1029   comparison.
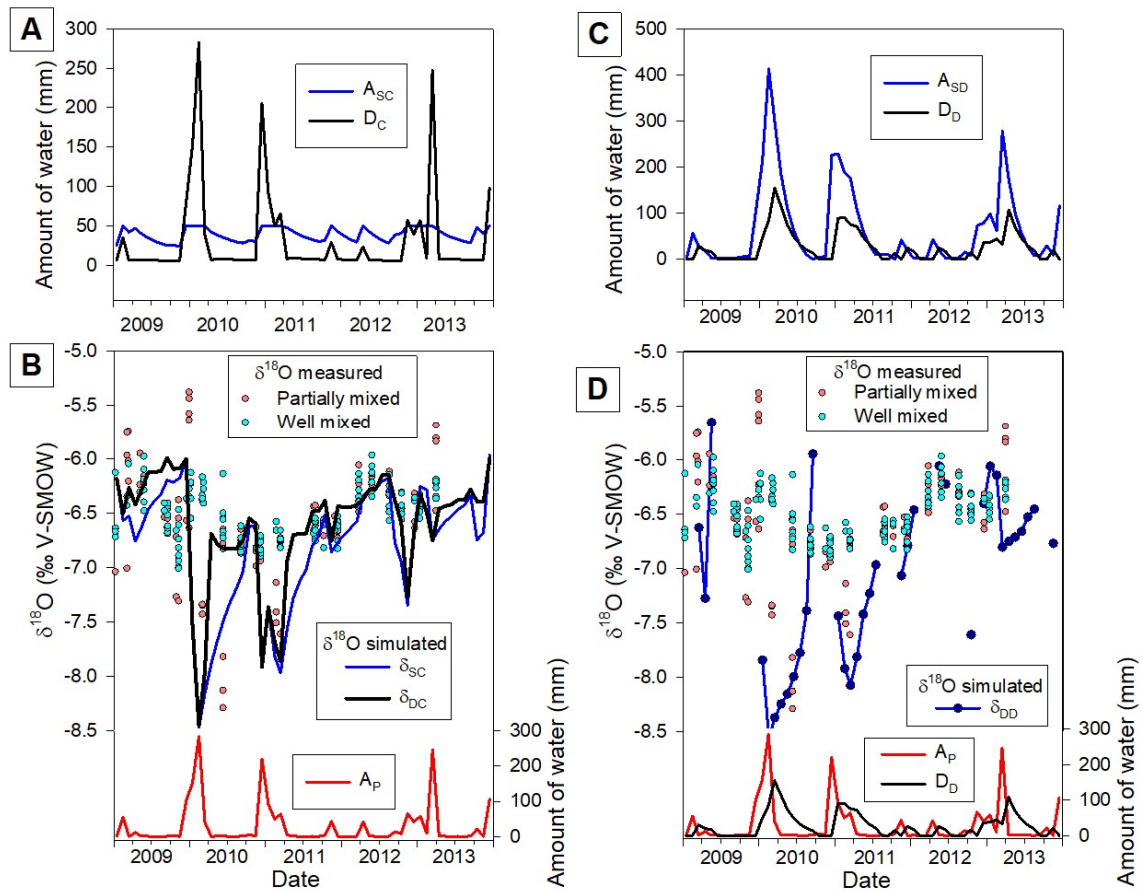
1030

1031

1032   Fig. 6. Simulations of drainages with preferential flow components in modules C and D.

1033   A) Main hydrological components of preferential flow in module C. A_{SC}: amount of water

1034   in the storage of module C, Q_C: discharge at drip site C. B) Simulated $\delta^{18}O$ signal of water

1035   in the storage C (δ_{SC}) and at the drip site C (δ_C). Observed $\delta^{18}O$ data are plotted for

1036   comparison. The amount of water provided by preferential flows (R_{TPf}) is plotted for

1037 comparison. C) Main hydrological components in module D. A_{SD}: amount of water in the

1038 storage of module D, Q_D: discharge at drip site D. D) Simulated $\delta^{18}O$ signal of water at

1039 the drip site D (δ_D). Observed $\delta^{18}O$ data are also plotted for comparison. The amount of

1040 water provided by preferential flows (R_{TPf}) and the discharge of drip D (Q_D) are plotted
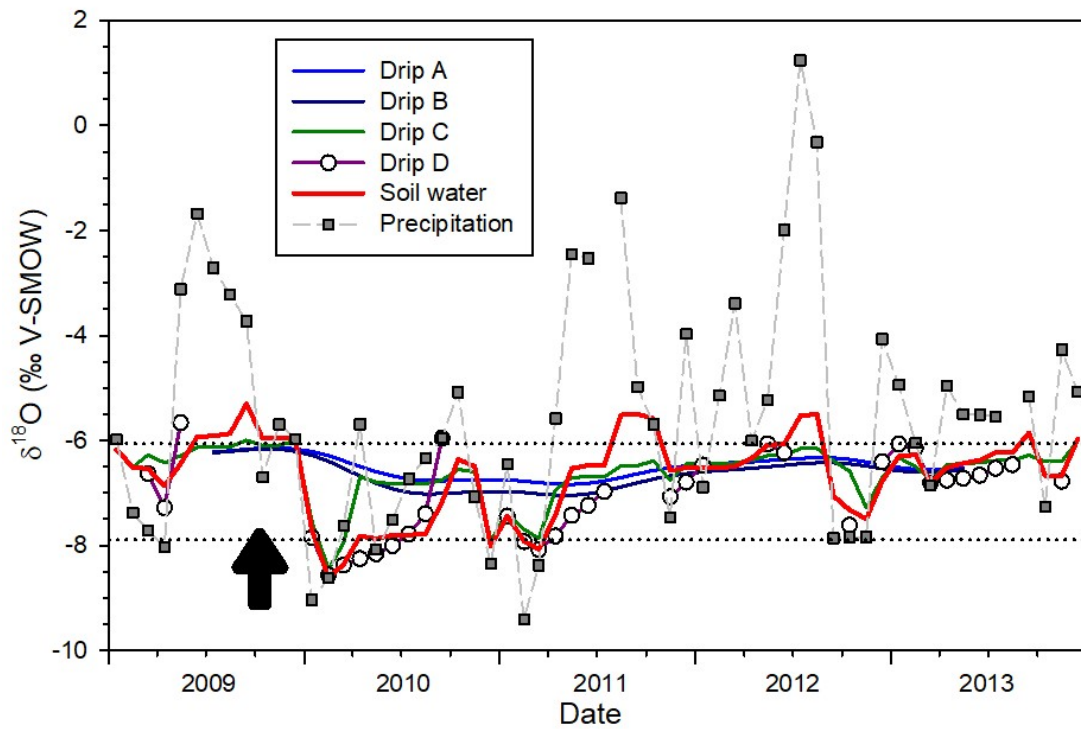
1041 for comparison.

1042

1043

1044

1045   Fig. 7. Comparison of simulated $\delta^{18}O$ signals of drips from modules A, B, C, and D with

1046   observed $\delta^{18}O$ records from sites classified into the four hydrological modules of

1047   ISODRIP. All partially-mixed waters were used to compare the simulations of drips C

1048   and D, although only those months with simulated discharge in drip D were used for

1049   comparison in the case of module D. For every month, observations of all drips

1050   characterized for a particular module were averaged. The vertical uncertainty bars

1051   accounts for two standard deviations of all observations for sites within each module and

1052   sampling campaign as well as the analytical error. The regression (blue dashed line) and

1053   the 95% confidence interval bands (grey lines) of the model-observation correlation are

1054   also plotted to evaluate the overlap of uncertainties. Clear outlier data from drips A and

1055   B (red crosses with their error bars) were removed from calculations (see supplementary

1056   material).

1057

1058

1059

Fig. 8. Drip and soil water $\delta^{18}O$ simulations. Monthly precipitation $\delta^{18}O$ record is displayed for comparison. Dotted horizontal lines represent the range of annually weighted $\delta^{18}O$ values of precipitation. The black arrow indicates the period that cause outliers in simulated drips A and B.

1064

1065